SCIENTIFIC REPORTS

OPEN

SUBJECT AREAS:
MAGNETIC PROPERTIES AND MATERIALS
NANOSCIENCE AND TECHNOLOGY
CONDENSED-MATTER PHYSICS

Received
28 November 2013

Accepted
22 July 2014

Published
3 September 2014

Correspondence and requests for materials should be addressed to E.D.T. (edt@gwu.edu)

* These authors contributed equally to this work.

Physical Justification for Negative Remanent Magnetization in Homogeneous Nanoparticles

Shuo Gu[1]*, Weidong He[2,3,4]*, Ming Zhang[5], Taisen Zhuang[6], Yi Jin[1], Hatem ElBidweihy[1], Yiwu Mao[7], James H. Dickerson[4,8,9], Michael J. Wagner[5], Edward Della Torre[1] & Lawrence H. Bennett[1]

[1]Department of Electrical and Computer Engineering, George Washington University, Washington, DC, 20052, USA, [2]School of Energy Science and Engineering, University of Electronic Science and Technology of China, Chengdu 611731, China, [3]Interdisciplinary Graduate Program in Materials Science, Vanderbilt University, Nashville, TN, 372345, USA, [4]Vanderbilt Institute for Nanoscale Science and Engineering, Vanderbilt University, Nashville, TN, 37235, USA, [5]Department of Chemistry, George Washington University, Washington, DC, 20052, USA, [6]Department of Mechanical and Aerospace Engineering, George Washington University, Washington, DC, 20052, USA, [7]Institute of Nuclear Physics and Chemistry, China Academy of Engineering Physics, George Washington University, Mianyang 621900, China, [8]Department of Physics and Astronomy, Vanderbilt University, Nashville, TN, 37235, USA, [9]Department of Chemistry, Vanderbilt University, Nashville, TN, 37235, USA.

The phenomenon of negative remanent magnetization (NRM) has been observed experimentally in a number of heterogeneous magnetic systems and has been considered anomalous. The existence of NRM in homogenous magnetic materials is still in debate, mainly due to the lack of compelling support from experimental data and a convincing theoretical explanation for its thermodynamic validation. Here we resolve the long-existing controversy by presenting experimental evidence and physical justification that NRM is real in a prototype homogeneous ferromagnetic nanoparticle, an europium sulfide nanoparticle. We provide novel insights into major and minor hysteresis behavior that illuminate the true nature of the observed inverted hysteresis and validate its thermodynamic permissibility and, for the first time, present counterintuitive magnetic aftereffect behavior that is consistent with the mechanism of magnetization reversal, possessing unique capability to identify NRM. The origin and conditions of NRM are explained quantitatively via a wasp-waist model, in combination of energy calculations.

NRM, also known as negative coercivity or inverted hysteresis loop, has been observed in heterogeneous thin films, and heterogeneous NP systems (with amorphous matrix, large particle size distribution or core shell structure) by various experimental techniques (e.g., Vibrating Sample Magnetometer, SQUID magnetometry, Alternating Gradient Force, Magneto-optical Kerr Effect and Hall probe imaging)[1–9]. In normal magnetic behavior the magnetization follows the applied field with a phase lag, whereas in magnetic systems that display NRM, the magnetization of the descending branch of the hysteresis loop becomes negative while the applied field is still positive. Models and theories have been proposed to explain the observed NRM. For example, NRM in Ag/Ni multilayer films[4] and granular (Ni, Fe)-SiO_2 films[5] was explained by magnetostatic interaction; NRM in YCo_2/YCo_2 ($Fe_{10}Ni_{90}/Fe_{10}Ni_{90}$) polycrystal bilayer films and CoNbZr (CoFeMoSiB) amorphous single layer films were explained by competing uniaxial (biaxial) and uniaxial anisotropies[10,11], which was later extended to competing cubic and uniaxial anisotropies[12,13]; NRM in Cr_2O_3 coated CrO_2 particles[14], and a randomly distributed Co NP system[15] was explained by dipolar interactions between ferromagnetic and superparamagnetic particles.

These previously proposed explanations attributed NRM to heterogeneous structural characteristics, such as heterogeneous layers or interfaces, or non-uniform chemical composition of the studied system, and, therefore, cannot be applied to a homogeneous nanostructured system. In addition, an agreement on the existence of NRM has not been unanimously reached, mainly due to the concern about its perceived violation of the first law of thermodynamics, and the lack of adequate rationalization and verification of the inverted hysteresis loop in the previous studies. A systematic in-depth investigation into the intriguing NRM phenomenon is still lacking.

In this paper, we verify the thermodynamic permissibility of the observed NRM, via detailed insight into the major hysteresis loops and first-order reversal curves (FORCs) of the studied system and confirm the existence of NRM with counterintuitive magnetic aftereffect behavior that is consistent with the magnetic reversal mech-

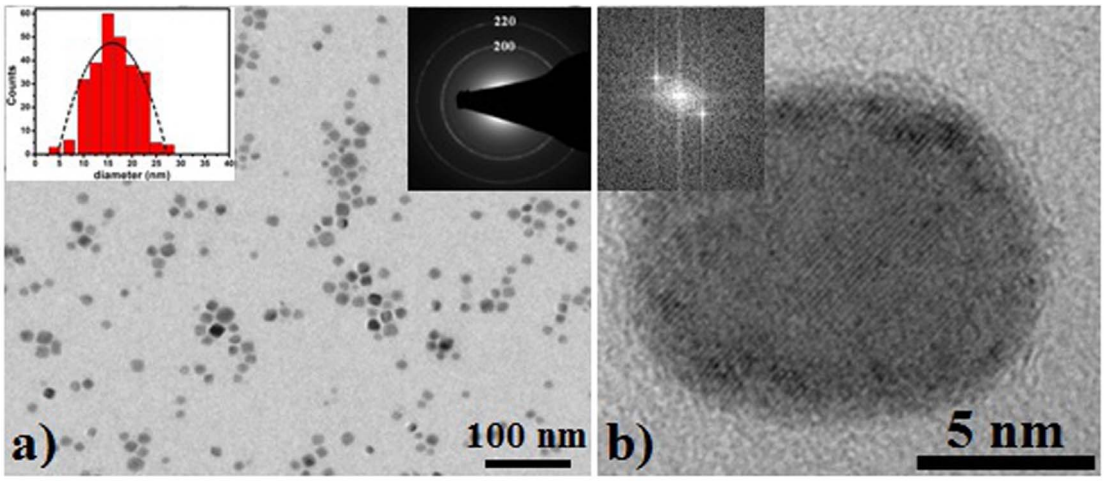

Figure 1 | Structural characterization of 15 nm EuS NPs. (a) HR-TEM micrograph of 15 nm EuS NPs (Insets: histogram of size distribution as fitted into function $y = -0.37x^2 + 11.78x - 46.41$, and an electron diffraction pattern of face-centered-cubic (fcc) EuS NPs, exhibiting features from arising from (220) and (200) lattice planes). (b) A high-magnification TEM image of a single EuS NP (Inset: electron diffraction pattern as obtained *via* Fourier analysis)[22].

anism. We further propose a novel interpretation of NRM as an extreme case of wasp-waist behavior[16] and present a quantitative explanation of the origin and conditions of NRM for simple nanomagnetic systems with uniform chemical composition and homogeneous structure. A three-dimensionally confined, matrix-free, nearly monodispersed EuS NP system is used to verify the presence of NRM in a simple homogeneous magnetic system. In contrast to direct exchange coupling in 3d ferromagnetic materials, (i.e., nickel, iron and cobalt), the magnetic properties of europium monochalcogenides (EuX: X = O, S, Se or Te) are caused by the half-filled 4f shell of the Eu^{2+} ions with a magnetic ground state $S_{7/2}$ and are jointly governed by ferromagnetic indirect exchange (J_1) among nearest neighbor Eu^{2+} ions and antiferromagnetic super-exchange (J_2) among next-nearest neighbor Eu^{2+} ions[17,18,19]. The behavior of EuX nanostructures, including the controversial NRM phenomenon observed in EuS NPs, is largely beneficial for the potential magnetic and optical applications of EuX crystals on the nanoscale[20–22].

Results

Structural characterization. The average size of the EuS NPs, employed in this study is 15 nm with less than 15% size distribution. A high-resolution transmission electron microscopy (HR-TEM) image and a selected area electron diffraction (SAED) pattern of the EuS NPs are shown in Fig. 1.

Magnetic characterization. Zero-field-cooled (ZFC) and field-cooled (FC) magnetization measurements from 2 K to 300 K were conducted for various field strengths from 20 Oe to 10000 Oe, (Fig. 2). When the field was reduced below 1000 Oe, a split between the ZFC and FC curves and the formation of a peak, at T_p, in the ZFC curves were observed. For $T < T_p$, the rotation of spins is frozen unless the external applied field is sufficiently large. As the temperature is increased in this range, the initial alignment of the spins, whose orientations were frozen when cooled to 2 K in the absence of an applied field is maintained and the increased

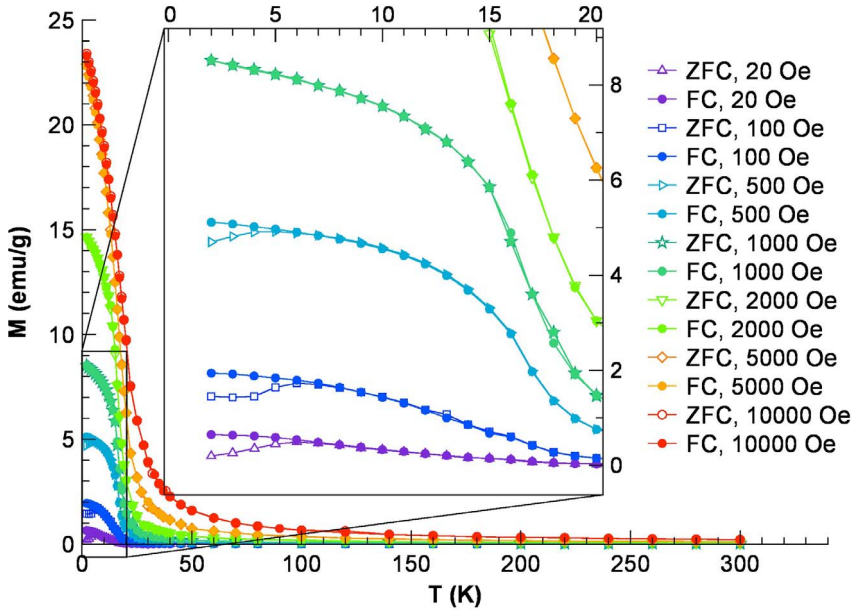

Figure 2 | The temperature dependence of the magnetization after zero-field-cooled and field-cooled magnetization using various field strengths from 20 Oe to 10000 Oe.

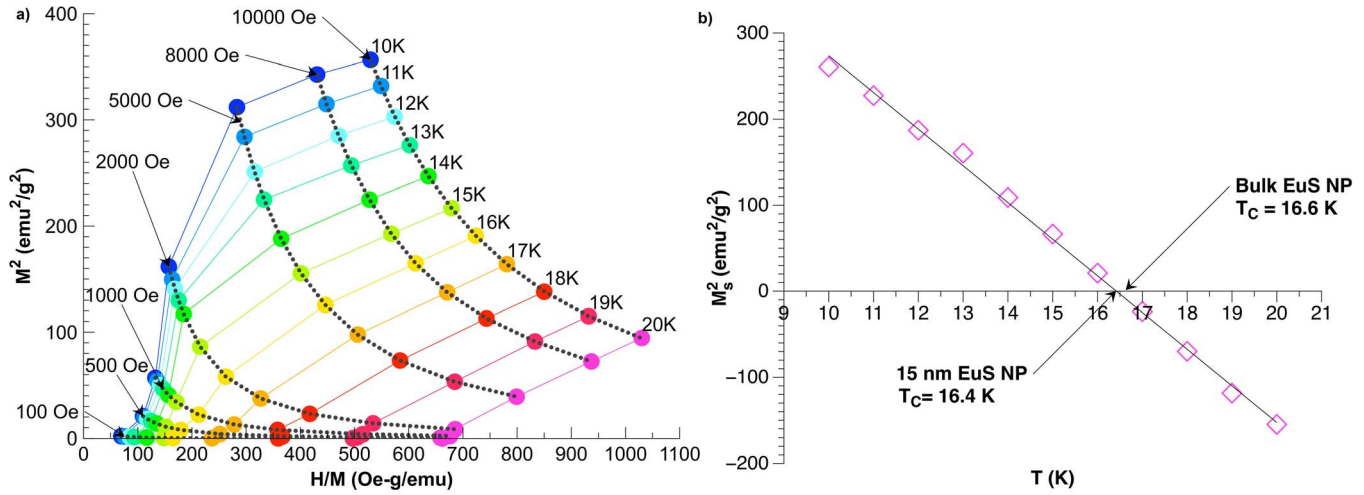

Figure 3 | Determination of T_C. (a) Arrot plots at temperatures between 10 K and 20 K. (b) M_s^2 vs. T plot from which T_C for 15 nm EuS NPs was determined. T_C for bulk EuS is indicated on the graph for comparison.

thermal fluctuation contributes to the increase in the magnetic moment by rotation of some spins that become free to align with the applied field. As the temperature increases above T_p, all of the spins became free to rotate. As a result, the magnetic moments decrease as the directions of spins becomes increasingly randomized due to thermal fluctuations. We must emphasize that T_p cannot be interpreted as a blocking temperature that marks the ferromagnetic to superparamagnetic transition, due to the existence of hysteresis at temperature significantly above T_p[23,24,25].

The Curie temperature, T_C, of the EuS NPs was determined from magnetization isothermals using an Arrott plot[26], i.e. a M^2 vs. H/M plot, as shown in Fig. 3a. The square of the spontaneous magnetization, M_s^2, was determined from the intercept of a linear extrapolation from the high field portion ($H > 5000$ Oe) of the isotherms to $H/M = 0$. A positive (negative) value of the intercept indicates that $T < T_C$ ($T > T_C$), i.e., the NPs are in ferromagnetic (paramagnetic) state. For the 15 nm EuS NPs, the positive (negative) value of the intercept were obtained from the isothermals at $T = 16$ K ($T = 17$ K); hence 16 K $< T_C <$ 17 K. The obtained M_s^2 values were then plotted as a function of T (Fig. 3b). The plotted points fall on a straight line with coefficient of determination, $R^2 = 0.9999$, and T_C, the temperature at which $M_s^2 = 0$, was determined for 15 nm EuS NPs to be 16.4 K, which is slightly lower than that of bulk EuS (16.6 K)[17]. Others have used isothermal measurements under applied fields up to 5000 Oe to evaluate T_C of 15 nm EuS NPs[27], however, our data indicate that isotherms measured in the vicinity of T_C continue to bend for applied fields higher than 5000 Oe, as shown in Fig. 3a. Extrapolations of the isothermals measured only up to 5000 Oe would place the evaluated T_C in an incorrect temperature range, i.e. 15 K $< T_C <$ 16 K. Hence, when the Arrott plot is applied, one must extrapolate from a sufficiently high field portion of the isotherms[28].

Magnetic hysteresis behavior. Major hysteresis loops were measured at temperatures in the range of 2 K to 300 K. The temperature dependence of remanent magnetization, M_r, is shown in Fig. 4. Positive remanent magnetization (PRM) and NRM were respectively observed in temperature ranges of 2 K $< T <$ 4.8 K and 4.8 K $< T <$ 25 K. As the temperature increased from 2 K, the magnitude of M_r reached zero at the reversal temperature, $T_r =$ 4.8 K, from a positive value, and the temperature at which hysteresis vanished, $T_{hv} = 25$ K, from a negative value. Zero magnitude of M_r persisted for temperatures above T_{hv}. Note: T_C is in the temperature range that exhibits NRM. M_r is determined by the magnetization of two sublattices that have different temperature characteristics. The occurrence of NRM is attributed to sufficient antiferromagnetic coupling between the sublattices.

For $T_r < T < T_{hv}$, the major hysteresis loops were partially inverted, with crossover between the descending and the ascending branch at a positive field and a negative field. For example, at 10 K, crossing between the descending branch and the ascending branch can be observed at 30000 Oe and −30000 Oe (Fig. 5). Insets (a) and (b) of Fig. 5 respectively show a high field region that displays normal hysteresis and a low field region that displays inverted hysteresis.

FORCs were measured, at various temperatures from 2 K to 300 K, to reveal elementary processes that cannot be sufficiently represented in major hysteresis loops and verify their thermodynamic permissibility. In FORCs measurements, a class of minor hysteresis loops was obtained by reserving the applied field at various points, H_r, on the descending (ascending) major hysteresis loop and subsequently going to positive (negative) saturation. For $T_r < T < T_{hv}$, the temperature range in which NRM is exhibited, the magnetization along the descending (ascending) branch of the major hysteresis loop is observed to be reversible for different H_r between the two crossover points.

We point out that the major hysteresis loop progressed in a normal counterclockwise direction; the occurrence of an apparent clockwise major and minor hysteresis loop in the inverted region, that might seem to be operating above unity efficiency, i.e. could be used to realize perpetual motion machines, violating the first law of ther-

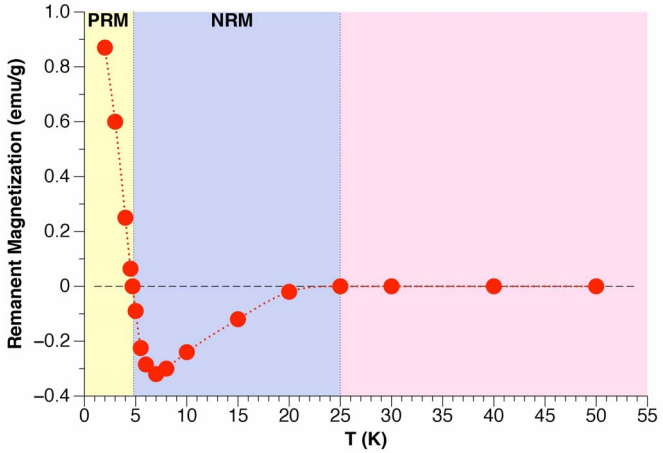

Figure 4 | The temperature dependence of the remanent magnetization.

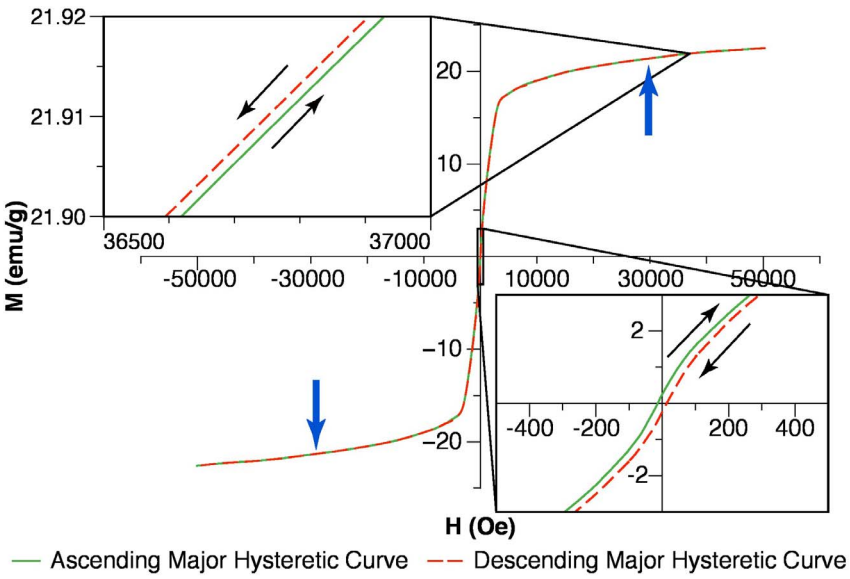

Figure 5 | **Major hysteresis loop measured at 10 K.** Insets: (Left) Detail of a high field region (36500 to 37000 Oe) that displays normal hysteresis. (Right) Detail of a low field region (−500 to 500 Oe) that displays inverted hysteresis.

modynamics, is actually due to the intersection of the descending and ascending branches of the counterclockwise major hysteresis loop. Remarkably, the observed partially inverted hysteresis loop is not real hysteresis behavior, but rather the joint behavior of the high-coercive surface spins and the low-coercive core spins of EuS NP, which will be discussed in detail. The reversibility in minor loops can only be observed while the applied field is not sufficiently high to switch the high-coercive component of magnetization. Energy over the entire loop is conserved; energy gain in inverted hysteresis in the low field region is compensated by the energy loss in normal hysteresis in the high field region. Hence, the observed partially inverted hysteresis loop is thermodynamically allowed, whereas a fully inverted hysteresis loop is not thermodynamically allowed, due to the inevitable energy loss in reversing the hard component of magnetization[29].

Magnetic aftereffect behavior. We report, for the first time, the unique capability of magnetic aftereffect experiments to identify the existence of NRM, and present the observation of an unusual magnetic aftereffect behavior of EuS NPs in the temperature range of $T_r < T < T_{hv}$ that is consistent with the mechanism of magnetization reversal. A typical magnetic aftereffect behavior of nanomagnetic materials that display a slow decay rate[30] is shown in Fig. 6a; the intensity of magnetization under a constant applied field decreases from its initial value, i.e. the magnetic moment on the descending hysteretic curve, towards its anhysteretic ground state with time. When the holding field is in the vicinity of the coercive field of the descending hysteretic curve, H_{Cd}, also known as the negative coercive field in typical hysteresis loop, the decay rate is maximized[31,32] and the initial magnetization is close to zero.

If NRM exists, i.e. $H_{Cd} > 0$, at a holding field that is close to H_{Cd}, the initial magnetization should be smaller in value than its corresponding anhysteretic ground state, and therefore the magnetic moment is expected to increase with time during thermal relaxation, as shown in Fig. 7.

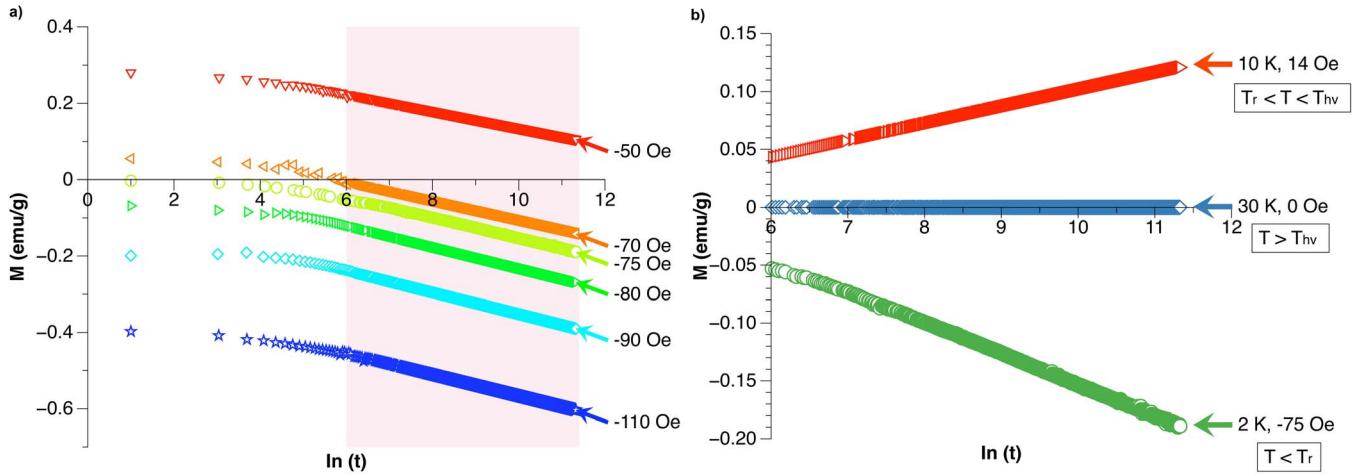

Figure 6 | **Magnetic aftereffect measurements.** (a) Magnetic aftereffect measured for 24 hours at 2 K for various holding fields in the vicinity of H_{Cd}. An analytical time window (ATW) from ~300 s to 24 hr, i.e. ln(t) from 6 to 11.4, were used in the measurements. Note: The first ~300 s were not included in the ATW to guarantee highly stable temperature and field values. In the selected ATW, the decay curves were observed to be quasi-linear and their slopes were used to determine the decay coefficient. (b) Comparison of magnetic aftereffect measured at 2 K, 10 K and 30 K for the holding fields of their respective H_{Cd}, −75 Oe, 14 Oe and 0 Oe, within the selected ATW.

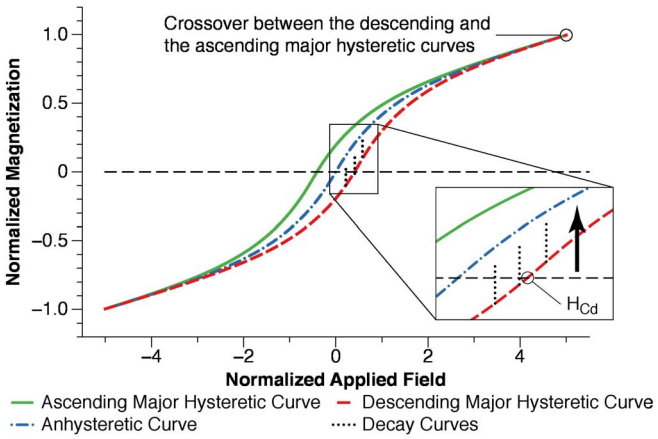

Figure 7 | Simulation of the descending and ascending major hysteretic curves and anhysteretic curve in the normalized field region of inverted hysteresis and the magnetic aftereffect decay curves for the holding fields in the vicinity of H_{Cd}. Inset: Detail of the magnetization decay from the initial magnetization on the descending hysteretic curve towards the anhysteretic curve (indicated by the arrow).

Figure 6b juxtaposes the magnetic aftereffect of 15 nm EuS NPs measured at three representative temperatures, 2 K, 10 K and 30 K, in the temperature range of $T < T_r$, $T_r < T < T_{hv}$, and $T > T_{hv}$, at the holding field of their respective H_{Cd}, i.e. −75 Oe, 14 Oe and 0 Oe. In contrast to the normal magnetic aftereffect behavior observed at 2 K ($T < T_r$), as expected, the magnetic moment increased with time at 10 K ($T_r < T < T_{hv}$). Therefore, the existence of NRM in homogeneous EuS NP system is confirmed and the consistency between the occurrence of NRM and the mechanism of magnetization reversal is validated.

Discussion

We propose that the NRM is an extreme case of wasp-waist behavior. In a typical wasp-waist hysteresis loop, the width of the loop narrows as the applied field goes to zero and then opens up[16]. A wasp-waist hysteresis loop can be generated if two ferromagnetic materials, one of which has a much larger coercivity than the other, are antiferromagnetically coupled.

Figure 8a shows an extreme case of the wasp-waist behavior. The hysteresis loops of the two ferromagnetic materials, with large and small coercivity, are respectively denoted as hard loop and soft loop. The saturation magnetization obtained in the soft loop, M_{soft}, is larger than that obtained in the hard loop, M_{hard}. We assert that when the above criteria are met, a wasp-waist hysteresis loop that exhibits NRM can be obtained. For given values of M_{hard} and M_{soft}, the shape of the obtained composite hysteresis loop can be adjusted to fit experimental data accurately by varying the exchange-coupling parameter, which is defined as the dimensionless ratio of the normalized equivalent field on one material by the normalized magnetic moment of the other material[33].

The energy per unit volume of the above described magnetic system that exhibits NRM can be given by

$$E = K\sin^2\beta_h + K_s\sin^2\beta_{s0} - M_hH\cos(\beta_h-\theta) - M_sH(\beta_s-\theta) - JM_hM_s\cos(\beta_h-\beta_s) \quad (1)$$

where the first two terms represent uniaxial anisotropy energy, the next two terms represent Zeeman energy, and the last term represents the exchange coupling between the hard and soft components. K is the anisotropy constant of the hard component, which can be determined from $2K/M = H_C$, and, K_s, the anisotropy constant of the soft component is assumed to be negligible, i.e. the system has single effective uniaxial anisotropy. J is the antiferromagentic exchange coupling constant. M_h and M_s are the magnetization of the hard and soft component. β_h and β_s are the angles between M_h and M_s and the easy axis of the hard component, and β_{s0} is the angle between M_s and the easy axis of the soft component. θ is the angle between the applied field and the easy axis of the hard component. A schematic illustration of the wasp-waist system, with the definition of parameters, is shown in Fig. 8b.

For the EuS NP system, enhanced or modulated physical characteristics, such as the magnetization[18,27,34–41], Curie/Neel temperature[18,36,37,39,40], Verdet constant[41,42], or absorption/luminescence/birefringence spectra[43–46], are observed compared to their bulk counterparts, often due to the contribution of uncompensated surface spins to the net properties (magnetization, for example) of the NP. Indeed, this has been observed when the nanocrystals' average diameter approaches a critical size[18,35,40,41,44,49]. As the size of EuS NPs is reduced to the nanoscale regime, the surface-to-volume ratio increase significantly and a bimodal magnetization state formed by surface spins and core spins, under certain temperature and field conditions, can be obtained[18,47–49]. Such characteristics could lead to a variety of nanomaterials applications, which could supplant those based on bulk EuS or on other magnetic materials[36,39,41,45]. The anisotropy energy of the three-dimensionally confined homogeneous EuS NP system is primarily attributed to the surface atoms, i.e., the anisotropy constant of the core atoms is assumed to be negligible. At saturation state, the magnetization of core atoms, M_{core}, are larger than that of the surface atoms, $M_{surface}$. In low energy regime, i.e. applied field and temperature are low, the core atoms and the surface atoms tend to align antiferromagnetically with each other. Hence, the EuS NP system meet the criteria of the wasp-waist system exhibiting NRM within appropriate window of related parameters, where the surface and core atoms can respectively be viewed as the hard and soft magnetization component.

The magnetization of the EuS NP system, which is the magnetization component of the net magnetization along the applied field, can be given by

$$M = M_{surface}\cos(\beta_{surface}-\theta) + M_{core}\cos(\beta_{core}-\theta) \quad (2)$$

where parameters denoted by subscripts surface and core are equivalent to those denoted by hard and soft in equation (1).

The magnetization reversal mechanism observed in EuS NPs is attributed to bimodal magnetization state formed by surface spins and core spins, which is due to evolving balance and changing dominance among anisotropy energy, Zeeman energy, and aniferromagnetic coupling energy under different field and temperature conditions[48].

When the applied field is sufficiently large, i.e., saturation field, both core spins and surface spins align along the applied field (Fig. 8c). In this case, Zeeman energy is dominant. While in low energy regimes, i.e., low temperature and low field, anisotropy energy is dominant and the surface spins can fluctuate along their easy axis. However, at very low temperature, i.e. 2 K $\leq T <$ 4.8 K, the antiferromagnetic coupling between the surface and core atoms are suppressed, because the rotation of core spins are frozen upon removal of the applied field, and mutual alignment of core spins is sustained in absence of external applied field. Within appropriate temperature window, i.e. 4.8 K $\leq T <$ 25 K, at the remanent state, core spins align antiparallel with the surface spin, i.e. easy axis, and the total magnetization is negative (Fig. 8d).

In summary, the NRM observed in a EuS NP system and simple nanomagnetic systems with uniform chemical composition and homogeneous structure, in general, has been rationalized. A wasp-waist model, in combination with energy calculations, is proposed to give unambiguous and quantitative explanations to the origin and conditions of NRM.

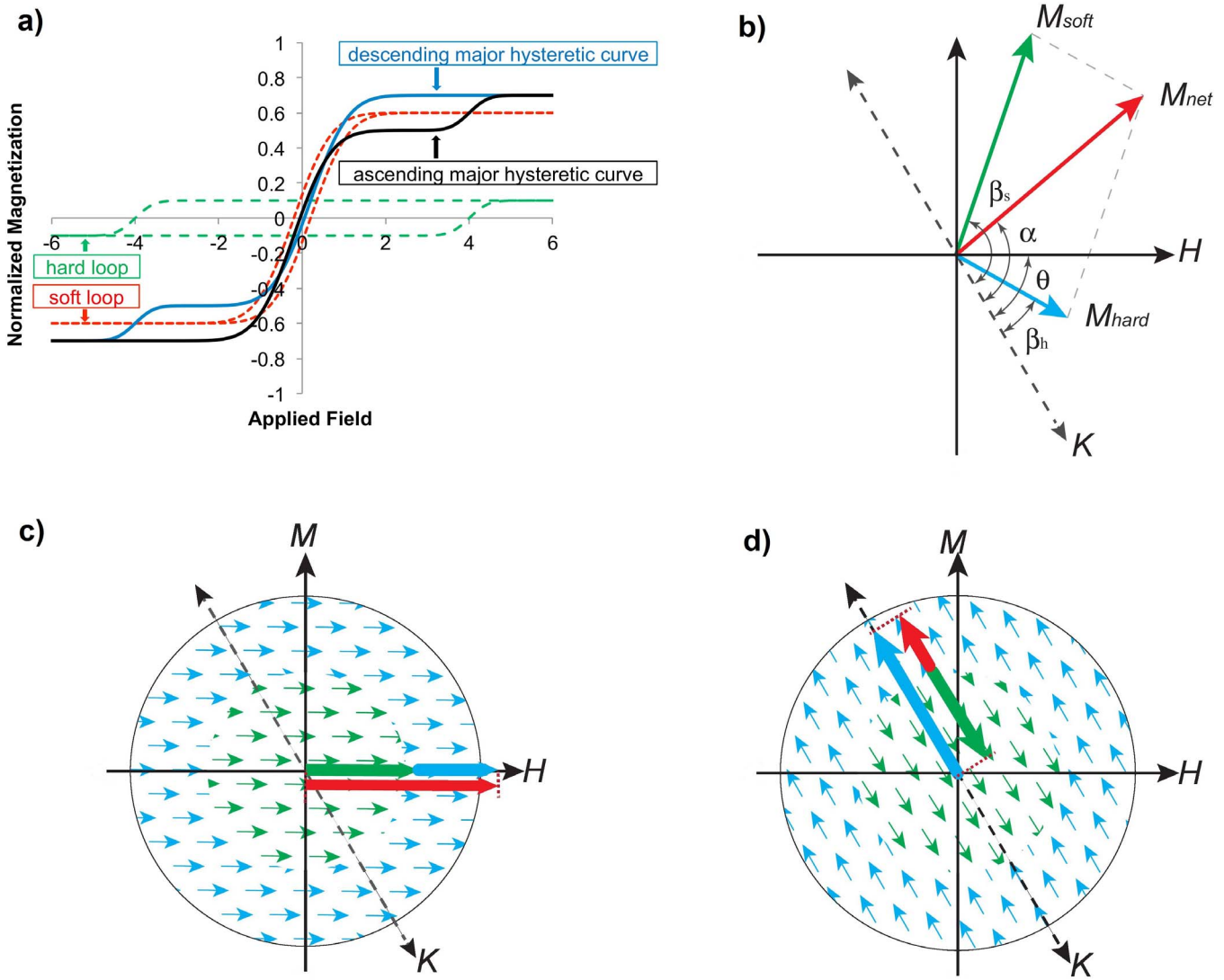

Figure 8 | Interpretation of the origin and conditions of NRM. (a) Illustration of an extreme case of wasp-waist behavior that exhibits NRM. (b) Schematic illustration of the proposed wasp-waist system. M_{soft}, M_{hard}, and M_{net} are respectively denoted by green, blue and red arrows. (c) Schematic illustration of a special case of spin orientation: both surface and core spins align along the field direction. Magnetization of surface and core spins is denoted by blue and green arrows, respectively. Total magnetization is denoted by red arrow. (d) Schematic illustration of a special case of spin orientation: the core (surface) spins align antiparallel (parallel) with respect to the easy axis and the total magnetization is negative. Magnetization of surface and core spins is denoted by blue and green arrows, respectively. Total magnetization is denoted by red arrow.

Methods

Sample preparation. Nearly monodispersed EuS NPs were colloidally synthesized using a one-step solvothermal synthesis technique[22,50,51]. The synthesis was carried out using a Schlenk line. 0.6 mmol of diethylammonium diethyldithiocarbamate, 0.2 mmol europium oleate, 0.6 mmol of phenanthroline, were dissolved in a solution of 1 ml of 1-dodecanethiol and 6 ml of oleylamine contained in a three-neck flask. The reaction mixture was then was degassed by purging at 80°C with argon flow for 45 min. Subsequently, the system was heated to 320°C under vigorous stirring. The reaction was allowed to proceed for 1 hour at 320°C, after which the mixture was transferred to a glass vial with a glass syringe. 10 mL acetone was added to the fresh purple EuS NP sample in oleylamine as synthesized. The sample was precipitated out on the bottom of the vial. The upper liquid was subsequently removed, and the EuS NPs were then cleaned with acetone for four times. The cleaned EuS NPs were dispersed in toluene for electron microscopic measurements.

Structural characterization. HR-TEM along with SAED pattern measurements were conducted using a Philips CM 200 operating at 200 kV. The sample for HR-TEM study was made by dropcasting of a EuS NP suspension in toluene onto carbon coated copper grids. The two dominant SAED ring patterns respectively correspond to (200) lattice plane and (220) lattice plane of FCC EuS NPs.

Magnetic characterization. Magnetic properties of the EuS NP system were studied using a SQUID magnetometer (Quantum Design, MPMS XL 5.0 Tesla). Major hysteresis loop and FORCs measurement protocols were adopted in characterization of magnetization as a function of applied field. In FORCs measurements, the magnetization was measured while the applied field was cycled between various H_r on the descending (ascending) major hysteresis loop and the positive (negative) saturation. ZFC and FC measurement protocols were adopted in characterization of magnetization as a function of temperature. In ZFC measurements, the EuS NPs were cooled in zero applied field to 2 K, and the desired applied field was applied, i.e. from 20 Oe to 10000 Oe. Magnetization was measured with ascending temperature to 300 K. FC measurements were conducted in a similar manner except that the EuS NPs were cooled in the presence of an applied field. In magnetic aftereffect measurements, the EuS NPs were first saturated by a large positive field, i.e. 50000 Oe, which is then rapidly decreased to a field in the vicinity of H_{Cd}, where it was held constant while the magnetization was measured as a function of time.

Modeling method. The major hysteresis loops and FORCs that correspond to the observed NRM was simulated as an extreme case of wasp-waist behavior using a Preisach model. In the Preisach model, the EuS NP was considered to be a parallel collection of independent squre-loop hysterons, where each hysteron is multiplied by a weight distribution function and then summed[32]. Characteristics of the hard and soft components within the Presiach model, i.e. hysterons that have high and low coercivities, can be respectively determined upon the identification of the Preisach parameters of the measured major hysteresis loops and FORCs.

1. Takanashi, K., Kurokawa, H. & Fujimori, H. A novel hysteresis loop and indirect exchange coupling in Co-Pt-Gd-Pt multilayers films. *Appl. Phys. Lett.* **63**, 1585 (1993).
2. Crisan, A., Pross, A., Humphreys, R. G. & Bending, S. Hall probe imaging of local hysteresisinversion and negative remanent fieldsnear the edge of a YBCO thin film. *Supercond. Sci. Technol.* **16**, 695–698 (2003).
3. O'Shea, M. J. & AlSharif, A. L. Inverted hysteresis in magnetic systems with interface exchange. *J. Appl. Phys.* **75**, 6673 (1994).
4. Dos Santos, C. A. & Rodmacq, B. Inverted and crossed hysteresis loops in Ag/Ni multilayers. *J. Magn. Magn. Mater.* **147**, L250 (1995).
5. Yan, X. & Xu, Y. Negative remanence in magnetic nanostructures. *J. Appl. Phys.* **79**, 6013 (1996).
6. Cougo dos Santos, M., Geshev, J., Schmidt, J. E., Teixeira, S. R. & Pereira, L. G. Origin of the magnetization reversal of an Fe thin film on Si(111). *Phys. Rev. B.* **61**, 1311–1314 (2000).
7. Long, J. G. *et al.* Magnetization property in Ta/NiFe/Ta sandwich structure. *J. Magn. Magn. Mater.* **226**, 1823–1824 (2001).
8. Wu, Y. Z., Dong, G. S. & Jin, X. F. Negative magnetic remanence in Co/Mn/Co grown on GaAs(001). *Phys. Rev. B.* **64**, 214406 (2001).
9. Ziese, M., Vrejoiu, I., Pippel, E., Nikulina, E. & Hesse, D. Magnetic Properties of $Pr_{0.7}Ca_{0.3}MnO_3$/$SrRuO_3$ Superlattices. *Appl. Phys. Lett.* **98**, 132504 (2011).
10. Valvidares, S. M., Álvarez-Prado, L. M., Martín, J. I. & Alameda, J. M. Inverted hysteresis loops in magnetically coupled bilayers with uniaxial competing anisotropies: Theory and experiments. *Phys. Rev. B.* **64**, 134423 (2001).
11. Valvidares, S. M. *et al.* Inverted hysteresis loops in annealed Co–Nb–Zr and Co–Fe–Mo–Si–B amorphous thin films. *J. Magn. Magn. Mater.* **169**, 242–245 (2002).
12. Arrott, A. S. *Nanomagnetism*. (Kluwer, Dordrecht, 1993).
13. Geshev, J., Viegas, A. D. C. & Schmidt, J. E. Negative remanent magnetization of fine particles with competing cubic and uniaxial anisotropies. *J. Appl. Phys.* **84**, 1488 (1998).
14. Zheng, R. K., Liu, H., Wang, Y. & Zhang, X. X. Inverted hysteresis in exchange biased Cr_2O_3 coated CrO_2 particles. *J. Appl. Phys.* **96**, 5370 (2004).
15. Yang, J. Y. *et al.* Inverted hysteresis loops observed in a randomly distributed cobalt nanoparticle system. *Phys. Rev. B.* **78**, 094415 (2008).
16. Bennett, L. H. & Della Torre, E. Analysis of wasp-waist hysteresis loops. *J. Appl. Phys.* **97**, 10E502 (2005).
17. Wachter, P. *Handbook on the Physics and Chemistry of Rare Earths*. (North-Holland, Amsterdam, 1979).
18. Redígolo, M. L. *et al.* Magnetization reversal in europium sulfide nanocrystals. *Appl. Phys. Lett.* **89**, 222501 (2006).
19. Silva, N. J. O., Millan, A. & Palacio, F. Remanent magnetization in CoO antiferromagnetic nanoaparticles. *Phys. Rev. B.* **82**, 094433 (2010).
20. Hasegawa, Y. *et al.* Remarkable magneto-optical properties of europium selenaide nanoparticles with wide energy gap. *J. Am. Chem. Soc.* **130**, 5710 (2008).
21. Schierle, E. *et al.* Antiferromagnetic Order with Atomic Layer Resolution In EuTe(111) Films. *Phys. Rev. Lett.* **101**, 267202 (2008).
22. Koktysh, D. S., Somarajan, S., He, W., Harrison, M. A., McGill, S. A. & Dickerson, J. H. EuS nanocrystals: a novel synthesis for the generation of monodisperse nanocrystals with size-dependent optical properties. *Nanotechnology.* **21**, 415601 (2010).
23. Rondinone, A, Samia, A. C. S. & Zhang, Z. J. Superparamagnetic Relaxation and Magnetic Anisotropy Energy Distribution in $CoFe_2O_4$ Spinel Ferrite Nanocrystallites. *J. Phys. Chem. B.* **103**, 6876–6880 (1999).
24. Nocera, T. M., Chen, J., Murray, C. B. & Agarwal, G. Magnetic anisotropy considerations in magnetic force microscopy studies of single superparamagnetic nanoparticles. *Nanotechnology.* **23**, 495704 (2012).
25. Crespo, P. *et al.* Permanent Magnetism, Magnetic Anisotropy, and Hysteresis of Thiol-Capped Gold Nanoparticles. *Phys. Rev. Lett.* **93**, 087204 (2004).
26. Arrott, A. & Noakes, J. E. Approximate equation of state for nickel near its critical temperature. *Phys. Rev. Lett.* **19**, 786–789 (1967).
27. Regulacio, M. D., Bussmann, K., Lewis, B. & Stoll, S. L. Magnetic Properties of Lanthanide Chalcogenide Semiconducting Nanoparticles. *J. Am. Chem. Soc.* **128**, 11173–11179 (2006).
28. Chiba, D., Fukami, S., Shimamura, K., Ishiwata, N., Kobayashi, K. & Ono, T. Electrical control of the ferromagnetic phase transition in cobalt at room temperature. *Nat. Mater.* **10**, 853–856 (2011).
29. Aharoni, A. Exchange anisotropy in films, and the problem of inverted hysteresis loops. *J. Appl. Phys.* **76**, 6977 (1994).
30. Gu, S., Jin, Y., Chen, P., Yan, C., Della Torre, E. & Bennett, L. H. Modeling of magnetic material displaying magnetic aftereffect with slow decay rates. *Physica B.* **407**, 1372–1376 (2012).
31. Wohlfarth, E. P. The coefficient of magnetic viscosity. *J. Phys. F: Met. Phys.* **14**, L155 (1984).
32. Della Torre, E., Bennett, L. H., Fry, R. A. & Ducal, Ó. A. Preisach–Arrhenius Model for Thermal Aftereffect. *IEEE Trans. Magn.* **38**, 3409–3416 (2002).
33. Della Torre, E. *Magnetic Hysteresis*. (Wiley-IEEE, Piscataway, 1998).
34. Kataoka, T., Tsukahara, Y., Hasegawa, Y. & Wada, Y. Size-controlled synthesis of quantum-sized EuS nanoparticles and tuning of their Faraday rotation peak. *Chem. Commun.* **48**, 6038–6040 (2005).
35. Thongchant, S., Hasegawa, Y., Wada, Y. & Yanagida, S. Size selective synthesis of surface-modified EuS nanocrystals using pyridine and their physical properties. *Chem. Lett.* **32**, 706–707 (2003).
36. Kar, S. *et al.* Gadolinium Doped Europium Sulfide. *J. Amer. Chem. Soc.* **132**, 13960–13962 (2010).
37. Selinsky, R. S., Han, J. H., Perez, E. A. M., Guzei, I. A. & Jin, S. Synthesis and Magnetic Properties of Gd Doped EuS Nanocrystals with Enhanced Curie Temperatures. *J. Amer. Chem. Soc.* **132**, 15997–16005 (2010).
38. Zhao, F., Sun, H. L., Gao, S. & Su, G. Magnetic properties of EuS nanoparticles synthesized by thermal decomposition of molecular precursors. *J. Mater. Chem.* **15**, 4209–4214 (2005).
39. Jung, J. *et al.* Europium-doped gadolinium sulfide nanoparticles as a dual-mode imaging agent for T-1-weighted MR and photoluminescence imaging. *Biomaterials* **33**, 5865–5874 (2012).
40. Zhao, F., Sun, H. L., Su, G. & Gao, S. Synthesis and size-dependent magnetic properties of monodisperse EuS nanocrystals. *Small* **2**, 244–248 (2006).
41. Thongchant, S. *et al.* First observation of Faraday effect of EuS nanocrystals in polymer thin films. *Jpn. J Appl. Phys. 2* **42**, L876–L878 (2003).
42. Hasegawa, Y. *et al.* Synthesis and photophysical properties of EuS nanoparticles from the thermal reduction of novel Eu(III) complex. *J. Phys. Chem. B* **110**, 9008–9011 (2006).
43. Chen, W., Zhang, X. & Huang, Y. Luminescence enhancement of EuS nanoclusters in zeolite. *Appl. Phys. Lett.* **76**, 2328–2330 (2000).
44. He, W. *et al.* Remarkable optical and magnetic properties of ultra-thin europium oxysulfide nanorods. *J. Mater. Chem.* **22**, 16728–16731 (2012).
45. Tsukahara, Y., Kataoka, T., Hasegawa, Y., Kaizaki, S. & Wada, Y. The first observation of the magnetic circular dichroism in EuS nanocrystals. *J. Alloys Compd.* **408**, 203–206 (2006).
46. Harrison, M. A. *et al.* Template assisted synthesis of europium sulfide nanotubes. *Mater. Lett.* **65**, 420–423 (2011).
47. Garanin, D. A. & Kachkachi, H. Surface contribution to the anisotropy of magnetic nanoparticles. *Phys. Rev. Lett.* **90**, 065504 (2003).
48. Kachkachi, H. & Mahboub, H. Surface anisotropy in nanomagnets: transverse or Néel?. *J. Mag. Mag. Mater.* **278**, 334 (2004).
49. Gambardella, P. *et al.* Giant Magnetic Anisotropy of Single Cobalt Atoms and Nanoparticles. *Science* **300**, 1130–1133 (2003).
50. Alivisatos, A. P. Semiconductor Clusters, Nanocrystals, and Quantum Dots. *Science.* **271**, 933–937 (1996).
51. Puntes, V. F., Krishnan, K. M. & Alivisatos, A. P. Colloidal nanocrystal shape and size control: The case of cobalt. *Science.* **291**, 2115–2117 (2001).

Acknowledgments

This research is partially supported by the US Department of Energy, Basic Sciences, Division of Materials Science and Engineering, Award DE-FG02-07ER46447; the National Science Foundation (NSF), Award DMR-0757380 and Award 1031619.

Author contributions

S.G. and W.H. designed and planned the study. S.G., W.H., Y.M. and J.H.D. conceived and carried out sample preparation and structural characterization. S.G., M.Z. and M.J.W. performed the magnetic characterization. S.G., W.H., M.Z., T.Z. and H.E. analyzed and interpreted experimental data with the help of all the other authors. S.G., Y.J. and E.D.T. performed numerical simulations and energy calculations. S.G. and W.H. wrote the manuscript with inputs from all authors. J.H.D., M.J.W., E.D.T. and L.H.B. supervised the study.

Additional information

Competing financial interests: The authors declare no competing financial interests.

How to cite this article: Gu, S. *et al.* Physical Justification for Negative Remanent Magnetization in Homogeneous Nanoparticles. *Sci. Rep.* **4**, 6267; DOI:10.1038/srep06267 (2014).